SUPPLEMENTAL INFORMATION FILE

Novel multiomics profiling of human carotid atherosclerotic plaques and plasma reveals BLVRB as a marker of intraplaque haemorrhage

- BLVRB is a marker of carotid atherosclerosis -

Ljubica Perisic Matic, PhD[1*], Maria Jesus Iglesias, PhD[2*], Mattias Vesterlund, PhD[3], Mariette Lengquist, BSc[1], Mun-Gwan Hong, PhD[2], Shanga Saieed, BSc[1], Laura Sanchez-Rivera, PhD[2], Martin Berg, MD[4], Anton Razuvaev, MD, PhD[1], Malin Kronqvist, BSc[1], Kent Lund, MD[1], Kenneth Caidahl, MD, PhD[1], Peter Gillgren, MD, PhD[5], Fredrik Pontén, MD, PhD[6], Mathias Uhlén, PhD[2], Jochen Schwenk M., PhD[2], Göran K. Hansson, MD, PhD[4], Gabrielle Paulsson-Berne, PhD[4], Erika Fagman MD, PhD[7], Joy Roy, MD, PhD[1], Rebecka Hultgren, MD, PhD[1], Göran Bergström, MD, PhD[8], Janne Lehtiö, PhD[3], Jacob Odeberg, MD, PhD[2, 4, 9#] and Ulf Hedin, MD, PhD[1#] ([*'#] Equal contribution)

[1]Department of Molecular Medicine and Surgery, Karolinska Institute, Stockholm, Sweden; [2]Science for Life Laboratory, Department of Proteomics, School of Biotechnology, Royal Institute of Technology, Stockholm, Sweden; [3]Department of Oncology-Pathology, Cancer Proteomics, Science for Life Laboratory and [4]Department of Medicine, Karolinska Institute, Stockholm, Sweden, [5]Department of Clinical Science and Education, Södersjukhuset and Department of Surgery, Södersjukhuset, Stockholm, Sweden; [6]Department of Immunology, Genetics and Pathology, Uppsala University, Uppsala, Sweden; [7]Department of Radiology and [8]Department of Molecular and Clinical Medicine, Sahlgrenska Academy, University of Gothenburg and Sahlgrenska University Hospital, Gothenburg, Sweden; [9]Coagulation Unit, Centre for Hematology, Karolinska University Hospital, Stockholm, Sweden

Materials and Methods

Ultrasound examination of patients and digital image analysis

For the evaluation of plaque density, records of the routine preoperative duplex examination were used. Examination records from n=95 patients were available for the analysis. From each exam one high-quality image of the plaques localized at the posterior wall of the carotid bifurcation at the area of maximal stenosis was selected for digital assessment. Images were imported into the Artery Measurement System (AMS) software for the analysis, as earlier described (1). Plaques were outlined manually and normalized using the lumen and adventitia as reference points. After the digital evaluation of plaque morphology, the relative size of the echolucent area was used for statistical analysis.

LC-MS/MS analysis and protein identification by HiRIEF

Samples were assigned to 4 TMT10 sets in order to minimize differences with regards to age, operating clinic, smoker status, calcification and symptom type. Each set contained 9 samples and 1 internal standard, which was set to channel 131. Central and distal peptide samples from 8 donors were utilized to generate the internal standard, which was identical for each set. To combine all 4 sets the TMT ratios were expressed as relative to the internal standard and median normalization was used to adjust for loading differences. 100 µg of peptides was labeled for all samples. Two of the sets contained central plaque tissues and two sets contained the corresponding distal (adjacent) tissues (e.g. channel 127C on set 1 contained the central part for donor X, and 127C in set 3 contained the distal part for the same donor). Asymptomatic patients were allocated to channels 126, 127N, 127C and 128N (for set 1 and 3) and to channels 126, 127N, 127C, 128N and 128C (for set 2 and 4). Samples from symptomatic patients were allocated to the remaining channels (128C/129N-130C).

TMT-labelled sample pools were subjected to peptide IEF-IPG (isoelectric focusing by immobilized pH gradient) in pI range 3-10 (300 µg). Freeze dried peptide samples were dissolved in 250 µL rehydration solution containing 8 M urea, 1% IPG Pharmalyte pH 3-10 and allowed to adsorb to the 24 cm linear gradient IPG strips (GE Healthcare) overnight and ran on an Ettan IPGphor 3 system (GE Healthcare) as described (2,3). After focusing, the peptides were passively eluted into 72 contiguous fractions through 3 elutions of MilliQ water, 35% Acetonitrile and 35% acetonitrile with 0,1% formic acid using an in-house constructed IPG extractor robotics (GE Healthcare Bio- Sciences AB, prototype instrument) into a 96-well plate (V-bottom, Corning product #3894), which were then dried in a

SpeedVac. The resulting fractions were freeze dried and kept at -20 °C. Online LC-MS was performed using a hybrid Q-Exactive mass spectrometer (Thermo Scientific). For each LC-MS/MS run, the auto sampler (Dionex UltiMate™ 3000 RSLCnano System) dispensed 15 µl of solvent A to the well in the 96 V plate, mixed, and proceeded to inject 7 µl. Samples were trapped on a C18 guard desalting column (Acclaim PepMap 100, 75um x 2 cm, nanoViper, C18, 5 µm, 100 Å), and separated on a 50 cm long C18 column (Easy spray PepMap RSLC, C18, 2 um, 100Å, 75 umx15cm). The nano capillary solvent A was 95% water, 5%DMSO, 0.1% formic acid; and solvent B was 5% water, 5% DMSO, 90% acetonitrile, 0.1% formic acid. At a constant flow of 0.25µl min^{-1}, the curved gradient went from 3%B up to 40%B in 50 min, followed by a steep increase to 100%B in 5 min.

FTMS master scans with 70,000 resolution (and mass range 300-1700 m/z) were followed by data-dependent MS/MS (35 000 resolution) on the top 5 ions using higher energy collision dissociation (HCD) at 30% normalized collision energy. Precursors were isolated with a 2m/z window. Automatic gain control (AGC) targets were 1e6 for MS1 and 1e5 for MS2. Maximum injection times were 100ms for MS1 and 150 ms for MS2. The entire duty cycle lasted ~1.5s. Dynamic exclusion was used with 60s duration. Precursors with unassigned charge state or charge state 1 were excluded. An underfill ratio of 1% was used.

Raw MS/MS files were converted to mzML format using msconvert from the ProteoWizard tool suite (4). Spectra were then searched using MSGF+ (v10072)(5) and Percolator (v2.08)(6), where 8 subsequent search results were grouped for Percolator target/decoy analysis. The reference database used was the human protein subset of ENSEMBL 75. MSGF+ settings included precursor mass tolerance of 10ppm, fully-tryptic peptides, maximum peptide length of 50 amino acids and a maximum charge of 6. Fixed modifications were TMT-10plex on lysines and N-termini, and carbamidomethylation on cysteine residues, a variable modification was used for oxidation on methionine residues. Quantification of TMT-10plex reporter ions was done using OpenMS project's IsobaricAnalyzer (v2.0) (7). PSMs found at 1% PSM- and peptide-level FDR (false discovery rate) were used to infer gene identities, and median normalization of ratios on the PSM level was performed. Protein level FDRs were calculated using the picked-FDR method (8).

Plasma antibody bead array assays

Polyclonal protein specific antibody reagents (n=10 260) were obtained from the Human Protein Atlas project (9). Antibodies were individually coupled to specific color coded magnetic beads (MagPlex®,

Luminex Corp) as previously described [10], which were combined to create a suspension bead array (SBA). Each SBA included four internal controls: beads with immobilised anti-human IgG (Jackson ImmunoResearch Lab) and anti-human albumin (Dako) as positive controls, while beads coupled with rabbit IgG from non-immunized rabbits (Bethyl) and beads without proteins immobilised served as negative controls.

Plasma samples were labeled as previously described [10]. Briefly, plasma was thawed on ice, randomized in a 96 well/plate and diluted 1:10 in 1x PBS buffer prior to the labeling process with ten-fold molar excess of biotin (Pierce). Biotinylated samples were further diluted 1:50 with PVXcasein assay buffer, heat-treated at 56°C for 30 min and incubated with 5 µl of the antibody SBA. After overnight incubation, beads were washed (PBS/0.05 % Tween-20) and the bound proteins cross-linked through addition of 0.4 % paraformaldehyde (PFA). Finally, streptavidin conjugated fluorophore (R-phycoerythrin, Invitrogen, SAPE diluted 1:750 in PBS-T) was added as detection reagent. The relative abundance of proteins was measured in FlexMap3D instrument (Luminex Corp.). The resulting median fluorescence intensity (MFI) per bead identity was used for data processing.

Sandwich immunoassays

A sandwich immunoassay (SIA) was developed using two antibodies generated towards two different regions of the BLVRB protein by the Human Protein Atlas project. HPA041937 was coupled to the Luminex beads and employed as capture reagent while HPA041698 was used as detection antibody, after biotin labeling as described previously (11). A commercial BLVRB antibody (#AF6568, Novus), with a confirmed high correlation index with HPA antibody (Supplementary Figure IVC), was also used for SIA in SCAPIS samples. Neat plasma samples were diluted 1:15 in assay buffer (PVXcasein) containing 10% rIgG (rabbit IgG), and heat-treated for 30 min at 56°C prior to incubation with the BLVRB bead array. After overnight incubation with rotation at room temperature (RT), unspecific proteins were removed by washing and the BLVRB biotinylated detection antibody was added at 1 µg/ml for 1.5 h. The beads were washed and incubated with SAPE for 30 min before a final wash and measured in the FlexMap3D instrument.

Immuno-capture mass spectrometry (IC-MS)

IC-MS was performed as previously described, with some modifications (12). In brief, 100 µL of pooled plasma from BIKE sample set was diluted, heated at 56°C and incubated overnight with beads covalently coupled to the anti-BLVRB HPA041937 antibody, or with normal rIgG as a negative

control. Each IC experiment was performed in triplicate. After trypsin digestion (enzyme:protein ratio 1:25), samples were analysed using a Q-Exactive HF (Thermo), equipped with an Ultimate 3000 RSLC nanosystem (Dionex). Raw data were queried against the Uniprot complete human proteome (version 20150521), using the Sequest engine under the platform Proteome Discoverer (PD, v1.4.0.339, Thermo Scientific). For IC, proteins identified were considered potential antibody targets if they fulfilled the following criteria: a peptide-spectrum match (PSM)>2 and identification in the 3 replicates. An internal database containing the most frequent proteins identified by IC-MS in control plasma was used to assign a z-score to each protein. A z-score of ≥4 was considered as cut-off to claim a protein as specifically enriched.

Immunohistochemistry (IHC)

All IHC reagents were from Biocare Medical (Concord, CA). Isotype rabbit and mouse IgG were used as negative controls. In brief, 5 µm plaque sections were deparaffinized in Tissue Clear and rehydrated in graded ethanol. For antigen retrieval, slides were subjected to high-pressure boiling in DIVA buffer (pH 6.0). After blocking with Background Sniper (Biocare Medical, BS966), primary antibodies: BLVRB (HPA041937), HMOX1 (ab12220, Abcam, Cambridge, UK) were diluted in Da Vinci Green solution (Biocare Medical, PD900), applied on slides and incubated at RT for 1h. For colocalisations, antibodies for cell-specific markers were used: von Willebrand factor (vWF, M0616, DAKO, Glostrup, Denmark,) CD4 (NCL-L-CD4368, Novocastra, Newcastle, UK) CD163 (ab74604, Abcam), CD8 (NCL-L-CD8295, Novocastra), CD68 (NCL-1-CD68, Novocastra), CD163 (MAB1652, Abnova) and smooth muscle α-actin (SMA, M0851, DAKO). A double-stain probe-polymer system containing alkaline phosphatase and horseradish peroxidase was applied, with subsequent detection using Warp Red (Biocare Medical, WR806) and Vina Green (Biocare Medical, BRR807A). The overlap between these two dyes resulting from close co-localisation of two proteins is observed as brown/grey signal. Slides were counterstained with Hematoxylin QS (Vector Laboratories, Burlingame, CA), dehydrated and mounted in Pertex (Histolab, Gothenburg, Sweden). The presence of ferric iron deposits was assessed by Perl's Prussian blue stain on adjacent serial plaque sections or fixed cells, performed using BIO-OPTICA kit (04-180807, Milano, Italy) according to the manufacturers' instructions, followed by counterstaining with nuclear Fast Red. Images were taken with a Nikon OPTIPHOT-2 microscope equipped with a digital camera and processed with NIS-Elements software.

Tissue microarrays (TMAs) and scoring of histological stainings

For generation of TMAs, plaques from n=106 additional patients were used and assembled as described previously (13). Tissue quality was assessed by Hematoxylin/Eosin staining, and areas with the least calcification were chosen. Three cores (1.5 mm x 5 mm) were punched from each plaque to compensate for the tissue heterogeneity. The individual cores were arrayed into recipient multicore TMAs, sectioned at 7 μm thickness and used for immuno-histochemical stainings. Blinded semi-quantitative evaluation of the TMA staining intensity (content) was performed according to a four-grade scale: 0 - no staining signal, 1 - weak signal or a few cells stained, 2 - medium or strong signal localized in a certain area, 3 - strong staining of the whole core section area.

Proximity Ligation Assay (PLA)

For proximity ligation assay, plaque slides were pretreated as for IHC. After blocking with Background Sniper, primary antibodies anti-BLVRB (HPA041937) and HMOX1 (ab12220) were diluted in Da Vinci Green solution, applied on slides and incubated at room temperature 1h in a humid chamber. PLA probe ligation and amplification steps were performed using Duolink In Situ Detection Brightfield kit (DUO 92012, Sigma-Aldrich), following manufacturers' instructions. Thereafter, slides were rehydrated in graded ethanol and mounted for visualization.

Iron stimulation assay

Human monocyte leukemia cell line THP1 (ATCC, TIB-202) was grown in suspension at 37°C in a humidified 5% CO_2 incubator in RPMI (Gibco, Life Technologies) medium supplemented with 2mM L-Glutamine, 10% FBS, 50 U/mL penicillin, and 50 μg/mL streptomycin. THP1 cells were seeded into polystyrene treated Falcon cell culture disposable dishes (Corning) and differentiated into macrophage-like cells by addition of Phorbol 12-myristate 13-acetate (PMA, Sigma, P8139) to a final concentration of 50 ng/ml for 72h (14). Cells were then stimulated with 100μM ferric ammonium citrate (FAC, RES20400-A702X, Sigma) in DMEM and samples collected after 2h, 4h, 8h, 24h and 48h. Non-stimulated cells were used as baseline controls at each time-point. Iron uptake in cells was demonstrated by Perl's blue staining and quantitated by using commercial colorimetric ferrozine-based assay (CFE-005, JAICA, Japan) (15).

Quantitative PCR

For quantitative PCR (qPCR), total RNA was reverse-transcribed using High Capacity RNA-to-cDNA kit (4387406, Applied Biosystems, Life Technologies, Carlsbad, CA). PCR amplification was done in

96-well plates in 7900 HT real-time PCR system (Applied Biosystems), using TaqMan® Universal PCR Master Mix (Applied Biosystems) and TaqMan® Gene Expression Assays (BLVRB Hs01106480_m1, HMOX1 Hs01110250_m1, Applied Biosystems). All samples were measured in duplicates. Results were normalized to the equal mass of total RNA as well as the Ct values of Ribosomal Protein Lateral Stalk Subunit P0 (RPLP0) housekeeping control (Hs99999902_m1). The relative amount of target gene mRNA was calculated by $2^{-\Delta\Delta Ct}$ method and presented as fold change compared to the baseline expression.

Immunofluorescence

Cells grown on glass coverslips were fixed in 4% PFA for 10 min at RT, permeabilized with 0.1 % Triton X-100/PBS for 5 min, followed by blocking with 2% normal goat serum/PBS for 1h. Cells were then incubated with primary antibodies diluted in the blocking solution for 3h at RT, washed with PBS and counterstained with Alexa Fluor 488 or 568-conjugated secondary antibodies for 1 h (Invitrogen). Nuclei were stained with diamidino-2-phenylindole (DAPI). For double labelling, incubations were performed sequentially to prevent cross-reactions. Images were taken using Zeiss LSM510 confocal microscope at 40x objective.

Bioinformatic and statistical analyses

Microarray and LC-MS/MS dataset analyses were performed with the GraphPad Prism 6 and Bioconductor software tools, using a linear regression model adjusted for age and gender and a two-sided Student's t-test assuming non-equal deviation. Statistical analysis of the Luminex data was performed in R. MFI was normalized using the Probabilistic Quotient Normalization (PQN) (16) and MA-loess normalization (17). All analyses were corrected for age, gender and multiple comparisons according to Bonferroni, while linear regression analyses were applied after confirming that statistical assumptions were satisfied. Group disease association analysis was performed using Wilcoxon signed rank sum test for paired samples and correlation coefficients were based on Spearman correlation. Spearman correlations were also calculated to determine the association between mRNA expression levels from microarrays (considered weak if $r<0.3$, moderate $0.3<r<0.6$ and strong $r>0.6$) and protein levels from LC-MS/MS. Genes belonging to the 'Hb degradation' and 'iron metabolism' pathways (n=22) were assembled from the Reactome database (http://www.reactome.org) and this list was further supplemented with their functionally related genes based on co-expression, co-interaction and shared biological function across tissues using the GeneMania (http://genemania.org) software (42 in

total). Enrichment analysis for gene ontology (GO) terms was performed on the whole set of 42 genes using Enrichr (http://amp.pharm.mssm.edu/Enrichr), GeneMania and Reactome software tools. Functional coupling network based on extended protein-protein interactions of BLVRB and HMOX1 was constructed using the FunCoup v.3.0 software (18). Functional information about individual genes was extracted from www.genecards.org. Survival analysis was done using the Cox regression model (19) with event-free survival as the response variable and log2-transformed gene expression levels as the explanatory variable. The covariates age and gender were tested and had no effect on results. Results were evaluated by Student's t-test, non-parametric Mann-Whitney test or group ANOVA when appropriate; p-value <0.05 was considered significant.

References

1. Ostling G, Persson M, Hedblad B, Goncalves I. Comparison of grey scale median (GSM) measurement in ultrasound images of human carotid plaques using two different softwares. Clin Physiol Funct Imaging 2013;33:431-5.

2. Eriksson H, Lengqvist J, Hedlund J et al. Quantitative membrane proteomics applying narrow range peptide isoelectric focusing for studies of small cell lung cancer resistance mechanisms. Proteomics 2008;8:3008-18.

3. Lengqvist J, Uhlen K, Lehtio J. iTRAQ compatibility of peptide immobilized pH gradient isoelectric focusing. Proteomics 2007;7:1746-52.

4. Kessner D, Chambers M, Burke R, Agus D, Mallick P. ProteoWizard: open source software for rapid proteomics tools development. Bioinformatics 2008;24:2534-6.

5. Kim S, Pevzner PA. MS-GF+ makes progress towards a universal database search tool for proteomics. Nature communications 2014;5:5277.

6. Kall L, Canterbury JD, Weston J, Noble WS, MacCoss MJ. Semi-supervised learning for peptide identification from shotgun proteomics datasets. Nature methods 2007;4:923-5.

7. Rost HL, Sachsenberg T, Aiche S et al. OpenMS: a flexible open-source software platform for mass spectrometry data analysis. Nature methods 2016;13:741-8.

8. Savitski MM, Wilhelm M, Hahne H, Kuster B, Bantscheff M. A Scalable Approach for Protein False Discovery Rate Estimation in Large Proteomic Data Sets. Molecular & cellular proteomics : MCP 2015;14:2394-404.

9. Uhlen M, Fagerberg L, Hallstrom BM et al. Proteomics. Tissue-based map of the human proteome. Science 2015;347:1260419.

10. Schwenk JM, Gry M, Rimini R, Uhlen M, Nilsson P. Antibody suspension bead arrays within serum proteomics. Journal of proteome research 2008;7:3168-79.

11. Dezfouli M, Vickovic S, Iglesias MJ, Nilsson P, Schwenk JM, Ahmadian A. Magnetic bead assisted labeling of antibodies at nanogram scale. Proteomics 2014;14:14-8.

12. Bruzelius M, Iglesias MJ, Hong MG et al. PDGFB, a new candidate plasma biomarker for venous thromboembolism: results from the VEREMA affinity proteomics study. Blood 2016.

13. Perisic L, Hedin E, Razuvaev A et al. Profiling of atherosclerotic lesions by gene and tissue microarrays reveals PCSK6 as a novel protease in unstable carotid atherosclerosis. Arteriosclerosis, thrombosis, and vascular biology 2013;33:2432-43.

14. Daigneault M, Preston JA, Marriott HM, Whyte MK, Dockrell DH. The identification of markers of macrophage differentiation in PMA-stimulated THP-1 cells and monocyte-derived macrophages. PloS one 2010;5:e8668.

15. Riemer J, Hoepken HH, Czerwinska H, Robinson SR, Dringen R. Colorimetric ferrozine-based assay for the quantitation of iron in cultured cells. Analytical biochemistry 2004;331:370-5.

16. Dieterle F, Ross A, Schlotterbeck G, Senn H. Probabilistic quotient normalization as robust method to account for dilution of complex biological mixtures. Application in 1H NMR metabonomics. Analytical chemistry 2006;78:4281-90.

17. Hong MG, Lee W, Nilsson P, Pawitan Y, Schwenk JM. Multidimensional Normalization to Minimize Plate Effects of Suspension Bead Array Data. Journal of proteome research 2016;15:3473-3480.

18. Schmitt T, Ogris C, Sonnhammer EL. FunCoup 3.0: database of genome-wide functional coupling networks. Nucleic acids research 2014;42:D380-8.

19. Folkersen L, Persson J, Ekstrand J et al. Prediction of ischemic events on the basis of transcriptomic and genomic profiling in patients undergoing carotid endarterectomy. Mol Med 2012;18:669-75.

Supplementary Tables

Supplementary Table I

GENERAL	Plasma cohort	Plaque proteomics cohort
number of patients	43	18
age (years, mean±SD)	72.49±8.01	71.85±2.63
gender (male/female)	33/10	18/0
BMI (mean)	26.32±3.80	26.15±1.14
smoking (present or former)	32 (74.4%)	11
SYMPTOMS		
asymptomatic	9	9
minor stroke (MS)	12	5
transitory ischemic attack (TIA)	11	2
amaurosis fugax (AF)	11	2
THERAPY		
lipid lowering medication (ezetimib, HMG-CoA reductase inhibitors)	40 (93%)	18 (100%)
antidiabetics	7 (16.27%)	4 (22.2%)
antihypertensives (ACE inhibitors, beta-blockers, diuretics, angiotensine II blockers)	31 (72%)	14 (77.7%)
COMORBIDITIES		
previous myocardial infarction	4 (9.3%)	4 (22.2%)
inflammatory diseases (rheumatoid arthritis, psoriasis, multiple sclerosis, inflammatory bowel disease)	4 (9.3%)	0
hypertension	31 (72%)	14 (77.7%)
diabetes	10 (23.26%)	4 (22.2%)
LAB MEASUREMENTS (mean±SD)		
serum creatinine (mg/dl)	85.86±24.39	89.34±7.67
serum cholesterol (mmol/l)	4.52±1.08	3.55±0.23
LDL (mmol/l)	2.64±1.06	1.80±0.20
HDL (mmol/l)	1.22±0.36	1.145±0.08
CRP (mg/l)	4.03±5.92	2.03±0.47
HbA1c (mmol/mol)	4.77±0.60	46.73±5.95
Hb (g/dl)	138.7±15.95	144.35±2.84

Supplementary Table I. Demographic characteristics of the BiKE discovery cohorts.

Supplementary Table II

Gene symbol	Gene name	Function
HP	haptoglobin	serine-type endopeptidase activity and hemoglobin binding
HBB	hemoglobin beta	iron ion binding and oxygen binding
HBA1	hemoglobin alpha 1	iron ion binding and oxygen binding
HBA2	hemoglobin alpha 2	iron ion binding and oxygen binding
HMOX1	heme oxygenase (decycling) 1	oxidoreductase activity, heme cleavage to form biliverdin
HMOX2	heme oxygenase (decycling) 2	heme oxygenase (decyclizing) activity
BLVRA	biliverdin reductase A	Reduces biliverdin to bilirubin with the concomitant oxidation of a NADH or NADPH cofactor
BLVRB	biliverdin reductase B (flavin reductase (NADPH)	Broad specificity oxidoreductase that catalyzes the NADPH-dependent reduction of a variety of flavin
UGT1A1	UDP glucuronosyltransferase 1 family, polypeptide A1	Enzyme that transforms lipophilic molecules, such as steroids, bilirubin into excretable metabolites
UGT1A4	UDP glucuronosyltransferase 1 family, polypeptide A4	This enzyme has glucuronidase activity towards bilirubin, but is more active on steroids and sapogenins
NOX1	NADPH oxidase 1	oxidoreductase activity and Rac GTPase binding
NOXO1	NADPH oxidase organiser 1	Constitutively potentiates the superoxide-generating activity of NOX1
NOXA1	NADPH oxidase activator 1	activates NADPH oxidases, enzymes which catalyze a reaction generating reactive oxygen species
POR	P450 (cytochrome) oxidoreductase	enzyme required for electron transfer from NADP to cytochrome P450 in microsomes
CYP2B6	cytochrome P450, family 2, subfamily B, polypeptide 6	enzyme involved in iron ion binding and NADPH-dependent electron transport pathway
CYP26A1	cytochrome P450, family 26, subfamily A, polypeptide 1	enzyme regulates the cellular level of retinoic acid which is involved in regulation of gene expression
TF	transferrin	transport of iron from sites of absorption and heme degradation to those of storage and utilization
TFRC	transferrin receptor	cell surface receptor necessary for cellular iron uptake by the process of receptor-mediated endocytosis
TFRC2	transferrin receptor 2	mediates cellular uptake of transferrin-bound iron
FTH1	ferritin, heavy polypeptide 1	Stores iron in a soluble, non-toxic, readily available form
HAMP	hepcidin antimicrobial peptide	hormone that constitutes the main circulating regulator of iron absorption and distribution across tissues
HPR	haptoglobin related protein	binds hemoglobin with high affinity and may contribute to the clearance of cell-free hemoglobin
MFI2	antigen p97 (melanoma associated)	shares sequence similarity and iron-binding properties with members of the transferrin superfamily
LTF	lactotrasferrin	major iron-binding protein in milk and body secretions with an antimicrobial activity
HBZ	hemoglobin, zeta	The zeta chain is an alpha-type chain of mammalian embryonic hemoglobin
HBD	hemoglobin, delta	Involved in oxygen transport from the lung to the various peripheral tissues
DHDH	dihydrodiol dehydrogenase (dimeric)	involved in the metabolism of xenobiotics by cytochrome P450 and porphyrin and chlorophyll
FTL	ferritin, light polypeptide	Stores iron in a soluble, non-toxic, readily available form
GFOD2	glucose-fructose oxidoreductase domain containing 2	has oxidoreductase activity and promotes matrix assembly
HBG1	hemoglobin, gamma A	The gamma globin genes (HBG1 and HBG2) are expressed in the fetal liver, spleen and bone marrow
GFOD1	glucose-fructose oxidoreductase domain containing 1	has oxidoreductase activity and promotes matrix assembly
HBQ1	hemoglobin, theta 1	found in human fetal erythroid tissue
HBE1	hemoglobin, epsilon 1	The epsilon chain is a beta-type chain of early mammalian embryonic hemoglobin
HBG2	hemoglobin, gamma G	The gamma globin genes (HBG1 and HBG2) are expressed in the fetal liver, spleen and bone marrow
HBM	hemoglobin, mu	iron ion binding and oxygen binding
HFE	hemochromatosis	regulates iron absorption by regulating the interaction of the transferrin receptor with transferrin
CYBA	cytochrome b-245, alpha polypeptide	Critical component of the membrane-bound oxidase of phagocytes that generates superoxide
FTHL17	ferritin, heavy polypeptide-like 17	primarily expressed in embryonic germ cells and binds iron but may lack ferroxidase activity
HMX1	H6 family homeobox 1	transcription factor involved in the development of craniofacial structures
NGB	neuroglobin	Involved in increasing oxygen availability and providing protection under hypoxic/ischemic condition
FTMT	ferritin mitochondrial	Stores iron in a soluble, non-toxic, readily available form
CYGB	cytoglobin	has a protective function during conditions of oxidative stress, involved in intracellular oxygen storage

Supplementary Table II. List of all candidates related to the GO categories ’Hb-degradation’ and ’iron metabolism’ and their functional annotations based on the GeneCards database.

Supplementary Table III

		Microarray plaques vs normal artery		Mass Spectrometry central vs peripheral plaque		Antibody bead array local vs peripheral plasma	
Gene symbol	Gene name	P-value	FC	P-value	FC	P-value	Antibody
HP	haptoglobin	ns	-	ns	-	na	-
HBB	hemoglobin beta	< 1E-04	88,12	2,28E-04	1,47	na	-
HBA1	hemoglobin alpha 1	ns	-	2,48E-04	1,47	na	-
HBA2	hemoglobin alpha 2	ns	-	nd	-	na	-
HMOX1	heme oxygenase (decycling) 1	< 1E-04	10,78	< 1E-04	1,43	na	-
HMOX2	heme oxygenase (decycling) 2	ns	-	ns	-	ns	HPA040611
BLVRA	biliverdin reductase A	< 1E-04	1,48	ns	-	ns	HPA042865/HPA054322
BLVRB	biliverdin reductase B (flavin reductase (NADPH)	< 1E-04	2,28	9,00E-03	1,28	4,68E-04/0.293	HPA041698/HPA041937
UGT1A1	UDP glucuronosyltransferase 1 family, polypeptide A1	ns	-	nd	-	na	-
UGT1A4	UDP glucuronosyltransferase 1 family, polypeptide A4	ns	-	nd	-	na	-
NOX1	NADPH oxidase 1	ns	-	nd	-	ns	HPA035299/HPA035300
NOXO1	NAPDH oxidase organiser 1	ns	-	nd	-	na	-
NOXA1	NAPDH oxidase activator 1	ns	-	nd	-	ns	HPA044781
POR	P450 (cytochrome) oxidoreductase	ns	-	ns	-	na	-
CYP2B6	cytochrome P450, family 2, subfamily B, polypeptide 6	ns	-	nd	-	na	-
CYP26A1	cytochrome P450, family 26, subfamily A, polypeptide 1	ns	-	nd	-	ns	HPA039317/HPA043953
TF	transferrin	ns	-	ns	-	na	-
TFRC	transferrin receptor	< 1E-04	2,04	ns	-	na	-
TFRC2	transferrin receptor 2	ns	-	nd	-	na	-
FTH1	ferritin, heavy polypeptide 1	< 1E-04	1,78	ns	-	na	-
HAMP	hepcidin antimicrobial peptide	< 1E-04	2,73	ns	-	na	-
HPR	haptoglobin related protein	1,74E-02	0,79	4,04E-03	1,39	na	-
MFI2	antigen p97 (melanoma associated)	< 1E-04	1,67	ns	-	ns	HPA004880
LTF	lactotrasferrin	< 1E-04	1,57	< 1E-04	1,88	na	-
HBZ	hemoglobin, zeta	ns	-	< 1E-04	1,35	na	-
HBD	hemoglobin, delta	< 1E-04	3,14	4,18E-03	1,34	na	-
DHDH	dihydrodiol dehydrogenase (dimeric)	ns	-	nd	-	na	-
FTL	ferritin, light polypeptide	< 1E-04	2,09	1,30E-03	1,37	na	-
GFOD2	glucose-fructose oxidoreductase domain containing 2	ns	-	ns	-	na	-
HBG1	hemoglobin, gamma A	ns	-	< 1E-04	1,54	na	-
GFOD1	glucose-fructose oxidoreductase domain containing 1	< 1E-04	0,62	ns	-	na	-
HBQ1	hemoglobin, theta 1	ns	-	1,02E-04	1,34	na	-
HBE1	hemoglobin, epsilon 1	ns	-	< 1E-04	1,94	na	-
HBG2	hemoglobin, gamma G	ns	-	< 1E-04	1,38	na	-
HBM	hemoglobin, mu	4,34E-03	1,33	nd	-	ns	HPA053951
HFE	hemochromatosis	< 1E-04	2,11	ns	-	ns	HPA053470
CYBA	cytochrome b-245, alpha polypeptide	< 1E-04	3,71	ns	-	ns	HPA045027
FTHL17	ferritin, heavy polypeptide-like 17	ns	-	nd	-	na	-
HMX1	H6 family homeobox 1	ns	-	nd	-	na	-
NGB	neuroglobin	1,71E-02	0,78	nd	-	ns	HPA042615
FTMT	ferritin mitochondrial	ns	-	nd	-	na	-
CYGB	cytoglobin	< 1E-04	1,49	nd	-	na	-

Supplementary Table III. Extended list of genes in the 'Hb degradation' and 'iron metabolism' GO categories examined in the large-scale profiles from BiKE patients. BLVRB was the only candidate consistently significantly upregulated in all 3 analyses. P-values corrected for multiple comparisons. ns-not significant; nd-not detected; na-not analysed; FC-fold change; FC > 1 upregulation, 0 < FC <1 downregulation.

Supplementary Figures

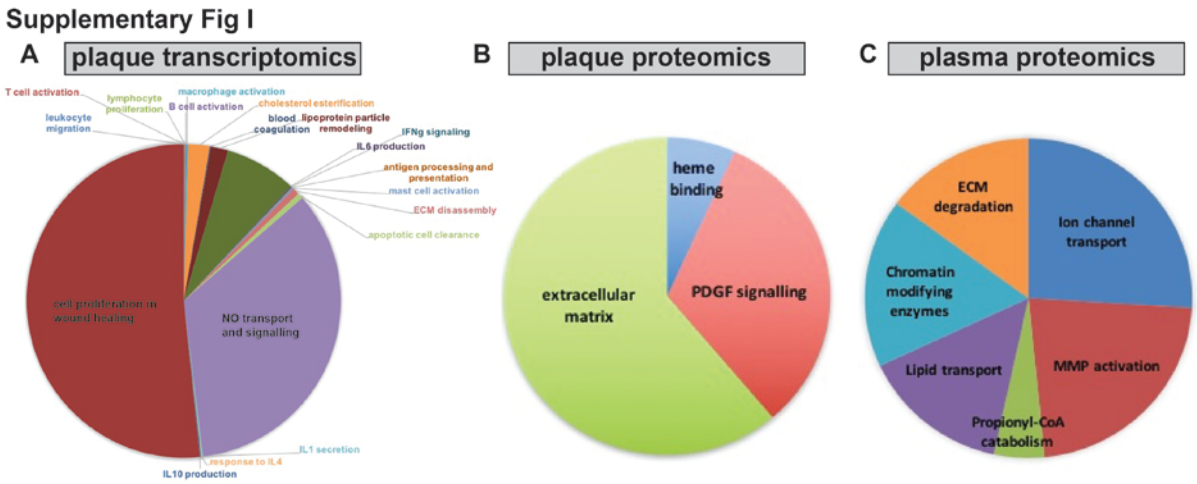

D **omics overlap, unfiltered**

		Microarray plaque vs normal artery		Mass Spectrometry central vs peripheral plaque		Antibody bead array local vs peripheral plasma	
Gene symbol	Gene name	P-value	FC	P-value	FC	P-value	direction
BLVRB	Biliverdin Beductase B	< 1E-04	2,28	0,00123	1,28	4,57E-08	upregulated
OLFML1	Olfactomedin Like 1	< 1E-04	1,5	0,03	0,8	0,00029	upregulated
CNN3	Calponin 3	< 1E-04	0,38	0,0124	0,82	0,00465	upregulated
MFAP4	Microfibril Associated Protein 4	0,0001	0,68	0,006	0,81	0,00594	upregulated
MCAM	Melanoma Cell Adhesion Molecule, CD146	< 1E-04	0,24	0.049	0,82	0,01027	upregulated
APOC1	Apolipoprotein C1	< 1E-04	39,37	<1E-04	1,43	0,01641	upregulated
MYH10	Myosin Heavy Chain 10	< 1E-04	0,33	0,0009	0,77	0,03490	upregulated

Supplementary Figure I. Pathway analyses of all differentially expressed transcripts and proteins in the 3 discovery omics datasets comparing plaques vs. normal arteries **(A)**, plaques vs. matched adjacent arterial tissues **(B)** and local vs. matched peripheral plasma **(C)**. Pie charts show enrichment of significant processes (all $p<0.05$). Table of candidates obtained by overlapping the 3 omics datasets **(D)**. FC-fold change; FC>1 upregulation; FC<1 downregulation.

Supplementary Figure II

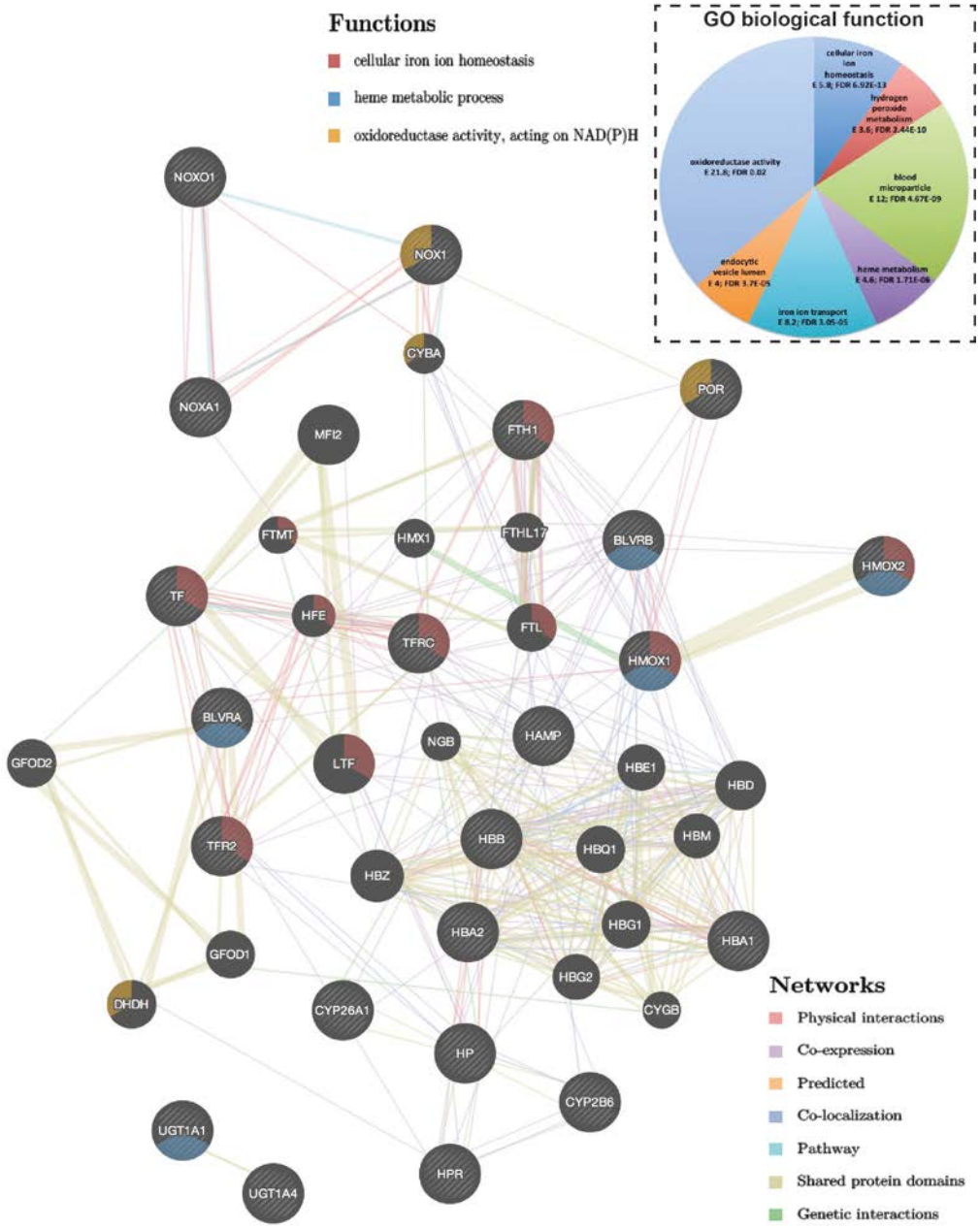

Supplementary Figure II. Functional coupling network of genes in the GO 'hemoglobin-degradation' and 'iron-metabolism' categories. Extended co-expression, co-localisation and co-interaction network of genes clustered in pathways related to intraplaque hemorrhage, was used for selecting candidates for further investigations. Network weighted for closeness in biological function based on publically available data; relations between genes shown by colored links (network legend). Dashed inset shows enrichment analysis of the genes in the network based on biological function. Network nodes belonging to the most significant categories are colored according to the functions legend. E-enrichment, FDR-false discovery rate.

Supplementary Figure III

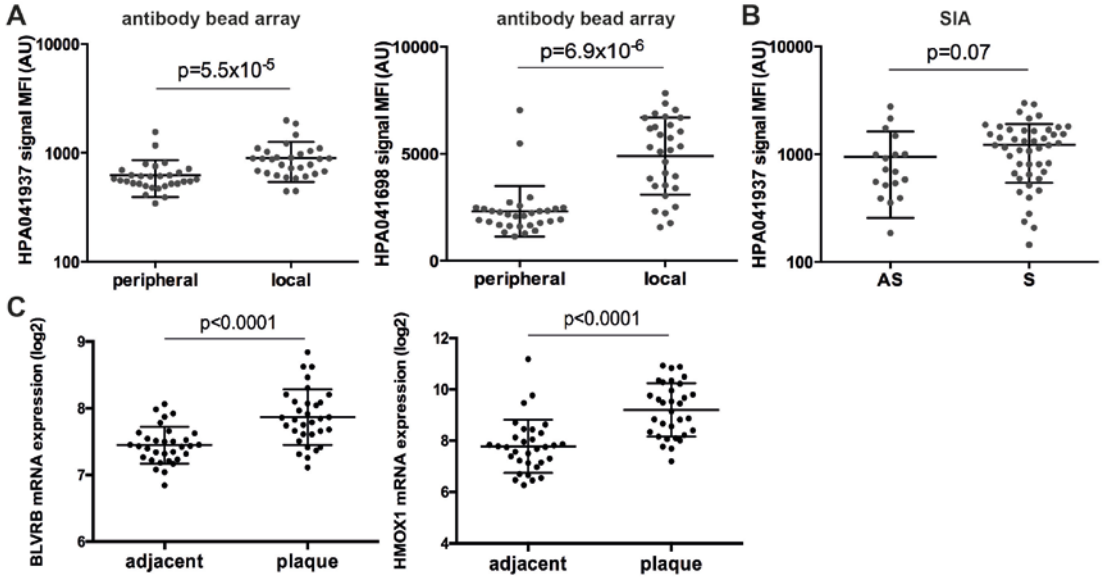

Supplementary Figure III. Significant enrichment of BLVRB in local compared to peripheral plasma was validated in another set of samples using antibody bead array where both HPA antibodies targeting BLVRB where included (n=33 patients, local vs. matched peripheral samples) **(A)**. BLVRB levels in plasma of symptomatic (S) patients were elevated compared to asymptomatic (AS) patients as shown by sandwich immunoassay in the validation cohort of n=66 patients (18 AS vs. 48 S) **(B)**. Plots show median of fluorescence intensity (MFI) with±standard deviation (SD). HMOX1 and BLVRB transcripts were upregulated in a publically available microarray dataset (GEO accession nr. GSE43292), comparing carotid plaques with adjacent arterial tissue (n=32 matched patient samples). Plots show log2 mean±standard deviation (SD) **(C)**.

Supplementary Figure IV

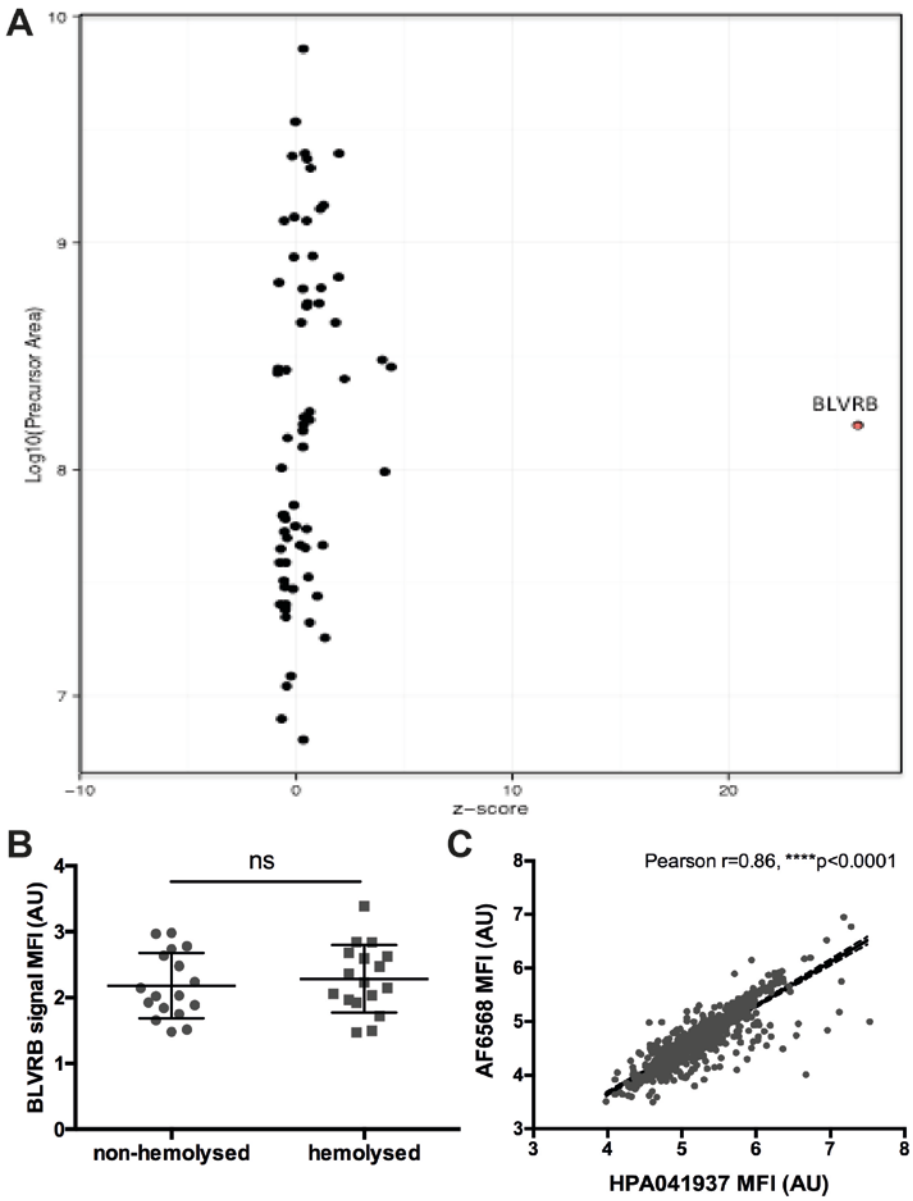

Supplementary Figure IV. Immuno-capture mass spectrometry analysis from a pool of plasma samples validated that HPA041937 primarily captured BLVRB and no other peptides were selectively enriched (z-score>4) **(A)**. BLVRB levels in association with hemolysis were assessed in additional plasma from normal individuals, by comparing samples that were mechanically hemolysed (sheared 3 times using a 5ml syringe and 23-gauge needle) with paired non-hemolysed ones. BLVRB levels were measured by sandwich immunoassay in n=17 peripheral plasma samples from normal individuals. Plot shows median of fluorescence intensity (MFI)±standard deviation (SD) **(B)**. Commercial AF6568 and HPA041937 antibodies show high correlation index for detection of BLVRB in peripheral plasma samples **(C)**.

Supplementary Figure V

A

Transcriptomic correlations

Gene name	Spearman r	P value	Significance
CD4	0.27	0.002	**
CD8	0.19	0.03	*
PECAM-1 (CD31)	0.52	<0.0001	****
vWF	0.39	<0.0001	****
MYH11	-0.53	<0.0001	***
ACTA2	-0.36	< 0.0001	****

Proteomic correlations

Protein name	Spearman r	P value	Significance
CD4	0.45	0.006	**
CD8	not detected		
PECAM-1 (CD31)	0.29	0.08	ns
vWF	0.04	0.82	ns
MYH11	-0.59	0.0001	***
SMA	-0.8	< 0.0001	****

B

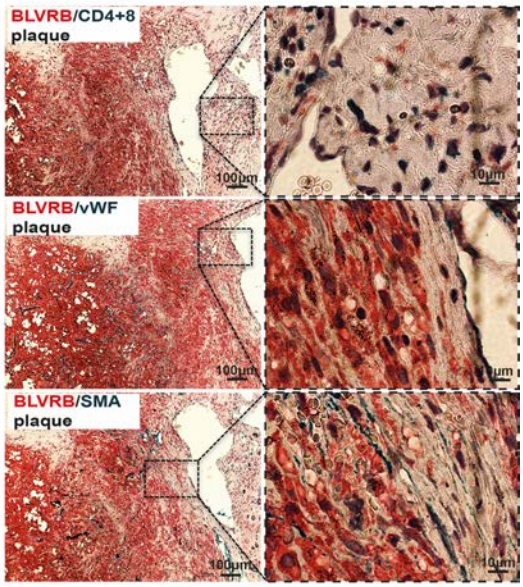

Supplementary Figure V. Weak to moderate correlations of BLVRB with markers of T-tymphocytes (CD4, CD8) and endothelial cells (vWF, PECAM1) were found in the transcriptomic and proteomic profiles from plaques, and inverse correlations with markers of smooth muscle cells (ACTA2, MYH11) **(A)**. By immunohistochemistry, BLVRB protein was sporadically localised to lymphocytes in plaques (dark brown overlap signal, enlarged images) **(B)**.

Supplementary Figure VI

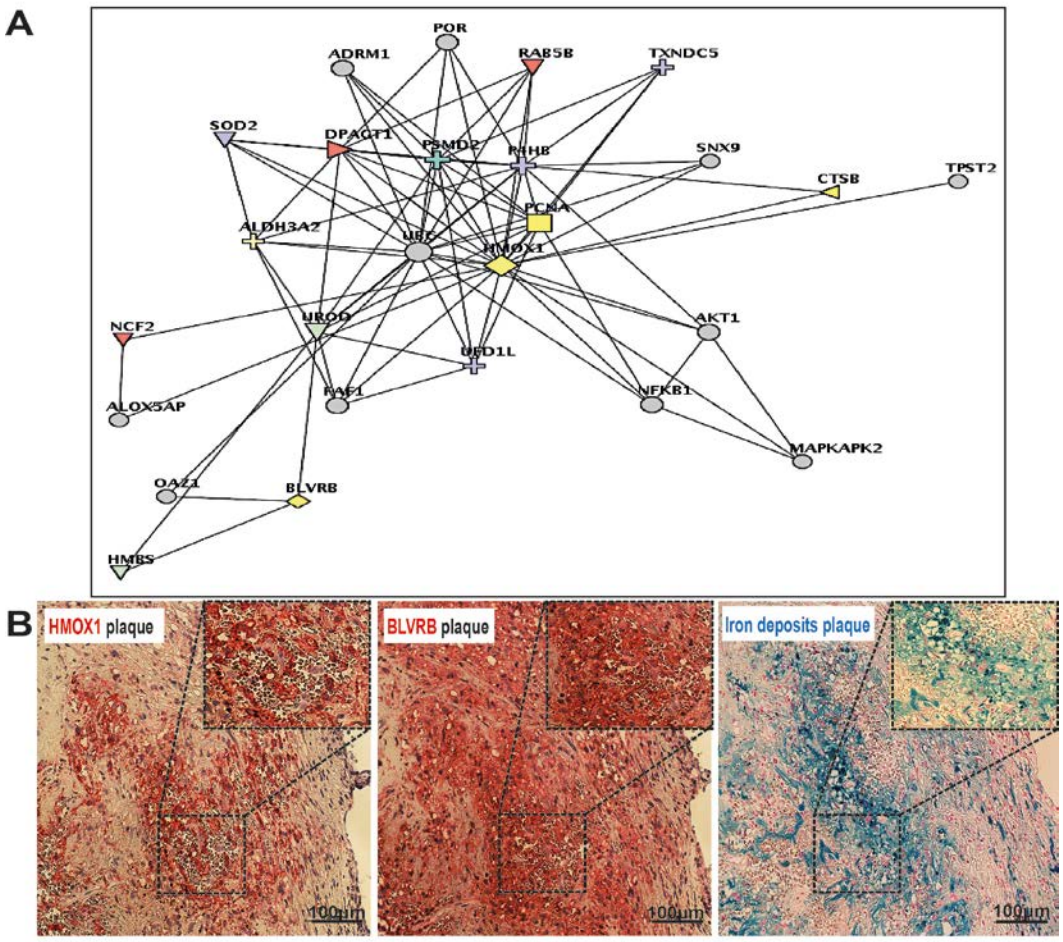

Supplementary Figure VI. Functional coupling network based on the known extended protein-protein interactions of BLVRB implicates this protein in the heme-catabolism cascade *via* HMOX1 **(A)**. Additional photomicrographs from consecutive plaque slides confirming BLVRB/HMOX1 co-localisation by immunohistochemistry (**B**, enlarged insets) in regions with IPH, as shown by Perl's blue staining.

Supplementary Figure VII

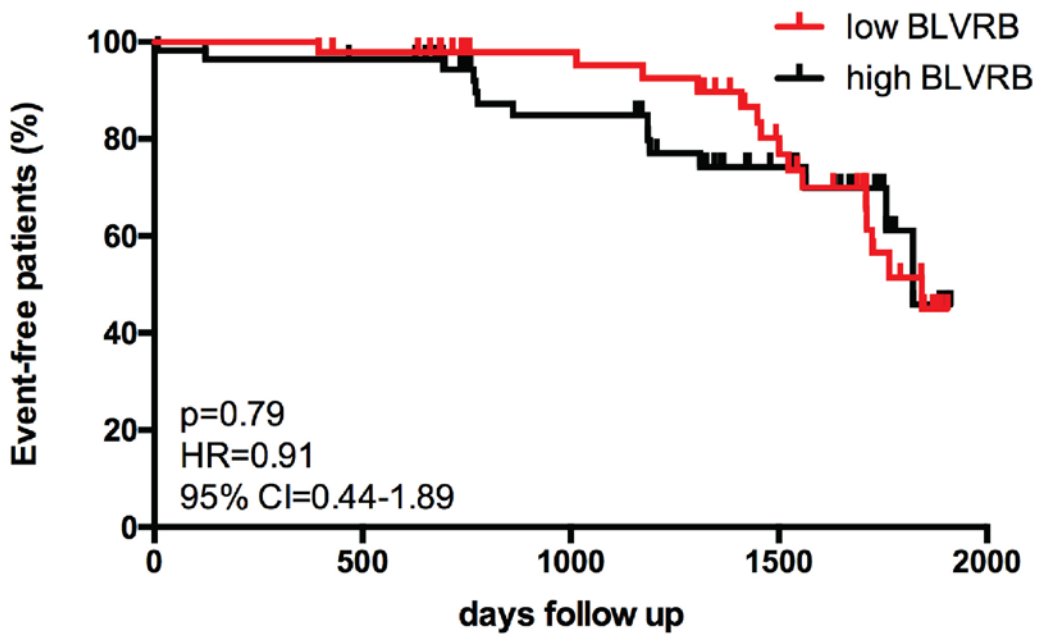

Supplementary Figure VII. Plot illustrating MACCE-free survival of patients during the 2000 days follow-up period after surgery, based on BLVRB mRNA expression in BiKE plaques above (black) and below (red) the median values (X-axis, days event-free survival). Hazard ratio (HR) refers to BLVRB high/low. Both symptomatic (n=86) and asymptomatic (n=40) patients were included in the analysis. Each mark along the lines indicates an event. Total number of events in the cohort was n=58.